Reaction Kinetics, Mechanisms and Catalysis (2025) 138:3159–3179
https://doi.org/10.1007/s11144-025-02874-4

Removal of methyl orange and methylene blue by both metallic (Ag, Cu) and bimetallic (Ag/Cu) nanoparticles: adsorption isotherms and kinetics

Burak Can Güney[1] · Ahmetcan Dikyar[1] · Muradiye Şahin[2] · Yasin Arslan[1]

Received: 13 March 2025 / Accepted: 27 May 2025 / Published online: 4 June 2025

Abstract

In this study, the adsorption of Methylene Blue (MB) and Methyl Orange (MO) dyes from aqueous solutions onto both metallic Ag NPs and Cu NPs and bimetallic Ag/Cu NPs obtained from the extract of Helichrysum arenarium, an aromatic plant, by green synthesis method was investigated and equilibrium isotherms and kinetic models were determined. The adsorption parameters, such as pH, adsorbent amount, contact time and initial concentration were optimized. The most successful removal for MO was achieved with Ag/Cu NPs at 76.9% under optimum conditions (20 mg/L MO, 20 mg Ag/Cu NPs, 60 min contact time, pH 2), while that for MB was achieved with Ag NPs at 82.7% under optimum conditions (20 mg/L MB, 20 mg Ag NPs, 60 min contact time, pH 4). Moreover, the adsorption data were modelled by Langmuir and Freundlich adsorption isotherms and Langmuir adsorption was found to be the most appropriate adsorption isotherm model for both MB and MO. Furthermore, while the pseudo-first-order reaction kinetic model was found to be the most suitable for MO dye, the pseudo-second-order reaction kinetic model was found to be the most suitable for MB dye. Based on the experimental results, bimetallic Ag/Cu NPs can be considered as effective, economic, and alternative adsorbent based on the maximum adsorption capacities which were found to be 191.696 mg/g for MO and 374.001 mg/g for MB. The highest efficiency of bimetallic Ag/Cu NPs is due to the properties of both Ag NPs and Cu NPs.

✉ Yasin Arslan
yasinarslan@mehmetakif.edu.tr

[1] Nanoscience and Nanotechnology Department, Faculty of Arts and Science, Burdur Mehmet Akif Ersoy University, Burdur, Turkey

[2] Kırşehir Ahi Evran University, Campus, 40100 Kırşehir, Turkey

Graphical abstract

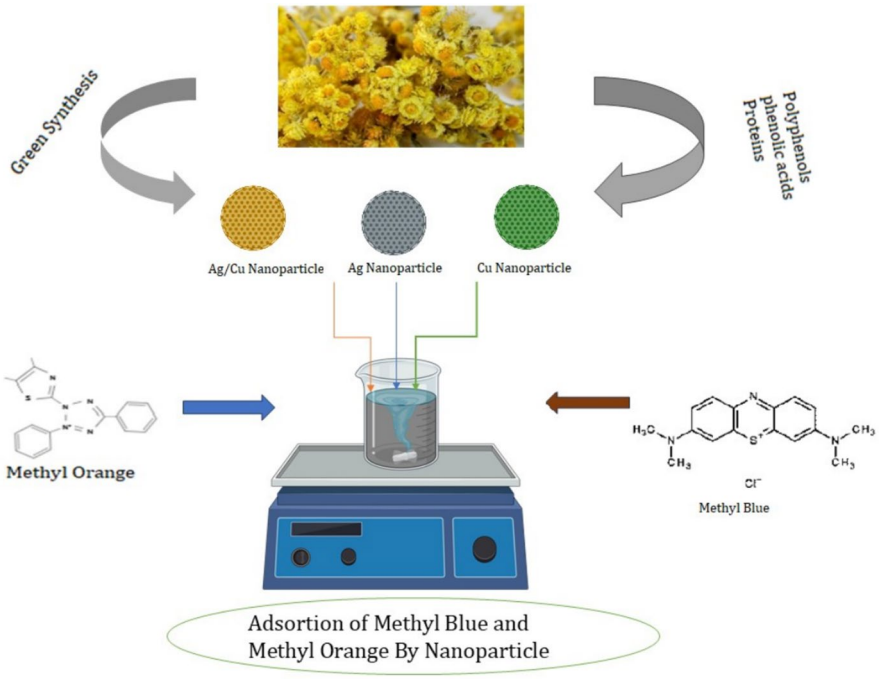

Keywords Green synthesis · Metallic nanoparticles · Adsorption · Adsorption isotherms · Kinetics

Introduction

Due to the complex molecular structures of dyes released into the environment from textile, chemical, pharmaceutical and dye industries, their removal can be conducted in a limited way in the wastewater. They also play a remarkably effective role in the possible water shortage in the future. Even in low concentrations, they can be extremely harmful to both environment and water ecosystems [1]. These dyes, which are widely found in industrial wastes, such as chemical, textile, pharmaceutical, and other areas, are carcinogenic, allergenic, mutagenic, toxic and highly resistant to biological degradation. To limit and reduce the toxic effects of these dyes on the environment and water ecosystem, different separation and purification methods have been applied and developed, including ozonation, ion exchange, precipitation, microbial separation, filtration, electrochemical methods and adsorption [2–4]. Among them, adsorption is frequently preferred due to its practicality and simplicity application, low cost, sensitivity to toxic substances, efficiency, and successful applicability at extremely low concentrations. In principle, adsorption efficiency is

related to pH, temperature, contact time, and other environmental parameters. In addition to the environmental conditions, the type of adsorbent used significantly affects the adsorption efficiency [4].

Urucu et al. investigated the degradation of Methylene Blue (MB) dye via phytoremediation with Juncus effusus plant. This study also involved the determination of associated degradation byproducts. Under optimized conditions, an experimental adsorption capacity was found to be 1.421 mg/g based on plant wet weight for MB [5]. Ihaddaden et al. conducted a study focused on achieving the highest removal rates for MB by utilizing coagulants derived from both Bentonite and Opuntia ficus indica. These natural coagulants were presented as ecological alternatives to conventional chemical coagulants. The removal efficiency was found to be 98.29% for MB [6]. Othmani et al. investigated the removal of MB and Methyl Orange (MO) dyes via a flocculation methodology employing cactus-derived formulations in conjunction with alum. The flocculants utilized were distinguished by their natural origin, stability, and environmentally benign profile, demonstrating synergistic compatibility with alum. This approach achieved 83% and 63% removal efficiencies for MB and MO, respectively [7]. Bani-Atta et al. investigated the photocatalytic degradation of MO and MB dyes. The photocatalytic activity, conducted under UV irradiation utilizing a Calcium–Polyoxometalate catalyst, demonstrated potential for the remediation of organic pollutants in industrial wastewater. The study achieved 81.21% and 25.8% removal efficiencies for MB and MO, respectively [8]. Majeed et al. investigated ascorbic acid as an environmentally friendly, edible, and effective photo-oxidative material for the degradation of MB. This study demonstrated that photo-oxidation utilizing ascorbic acid achieved a 95% removal efficiency for MB revealing its significant potential for the remediation of toxic dye contaminants [9].

Due to superior functionality and suitability for modifications, homogeneous surface structure and large surface area, nanoparticles have found many applications, such as purification, catalysis, drug delivery, humidity control, heavy metal/dye adsorption and separation-purification processes, and are increasingly used especially for purifying dyes found in the wastewater [10].

The most key features of nanoparticles obtained by modification of metals are that their sizes and shapes can be adjusted depending on the synthesis conditions. The biological, physical, and chemical activities of nanoparticles depend on the size, shape, chemical composition, redox potential, particle dissolution, ion release, coating, and aggregation degree of nanoparticles. In addition, the available surface area and surface charge of nanoparticles play a significant role in this interaction [4, 10]. Nanoparticles are effective even at exceptionally low concentrations and minimize the possibility of toxicity. However, it has been shown that the current potential toxicity of nanoparticles is not only related to metal accumulation, but also to the methods used in the synthesis of nanoparticles. The use of toxic chemicals for traditional nanoparticle synthesis limits the applicability of nanoparticles. Since this situation increases the need to develop environmentally friendly alternative methods without using toxic substances, green synthesis has begun to be used. Green synthesis is more beneficial than conventional chemical synthesis methods because it is economic, reduces environmental pollution and increases the human health and

environmental safety. Green synthesis has been frequently preferred in recent years because it eliminates the use of expensive chemicals and is environmentally friendly [4, 10, 11].

Green synthesis, which is a method for the synthesize of both metallic and bimetallic nanoparticles that are biocompatible and suitable for modification with naturally obtained extracts, has begun to be widely used. With respect to chemically obtained nanoparticles, the metallic/bimetallic nanoparticles obtained by green method is being economical, biocompatible and have the non-toxicity of the by-products produced during production [12]. By using the green synthesis method, metallic nanoparticles, such as Ag, Au, Cu, Zn and bimetallic nanoparticles such as Ag/Cu, Au/Ag, Au/Cu, and metal oxide nanoparticles can be synthesized. The nanoparticles synthesized with this method find applications in agriculture, pharmacy, medicine and chemistry. In addition, these nanoparticles obtained show antioxidant, antimicrobial, and anticancer properties [12, 13].

Fungi, bacteria, algae, and plants are used as electron donors in nanoparticle synthesis with the green synthesis method. Fungi serve as particularly good biological agents in the synthesis of nanoparticles thanks to the enzymes that they contain. In general, larger amounts of nanoparticles have been synthesized by using fungi compared to bacteria. Bacteria are important biosynthesis tools in the green synthesis of nanoparticles. Different bacterial species can be used in the synthesis of nanoparticles. The most used species are both prokaryotic bacteria and actino bacteria. The use of algae in the synthesis of nanoparticles is not common. However, algae are also used in green synthesis with the functional groups they contain such as amine and hydroxyl [14].

Plants are mostly used in the green synthesis of nanoparticles compared to fungi, algae, and bacteria. When the studies are examined, it is seen that all parts of plants, such as stems, roots and leaves are used in the green synthesis of nanoparticles. In addition to the terpenoids, polysaccharides, phenolics, alkaloids, flavones, amino acids, enzymes, and proteins that they contain, plants provide rapid and safe nanoparticle synthesis thanks to the bioactive components, such as chlorophyll pigments, caffeine, eugenol, ascorbic acid, and theophylline [13]. The use of plants and their extracts in green synthesis attracts attention due to reasons, such as their rapid growth, easy accessibility, ability to perform nanoparticle synthesis in a single step and economically, non-pathogenicity and environmental friendliness. Recently, metallic, bimetallic, and metal oxide nanoparticles are frequently preferred as adsorbents in adsorption studies conducted for the removal of dye pollutants. Aromatic plants are plants with different uses in industries, such as chemistry, medicine, pharmaceuticals, food, and cosmetics, and it is known that they have been used for such purposes since the beginning of human history [13, 15].

The aromatic plants are obtained from nature, while some are produced by taking them under special conditions specific to distinct cultures. One of the important purposes of using aromatic plants that are the subject of research is their use for obtaining extracts for nanoparticle production by green synthesis method. *Helichrysum arenarium* is a perennial aromatic plant that grows in rocky areas with yellow flowers between 50 and 60 cm in height. The extract of *Helichrysum arenarium* has many biological activities, such as antiviral,

antimicrobial, antibacterial, antioxidant, anti-inflammatory, antifungal, antiproliferative, antiallergic, antiradical, cholinergic, hepatoprotective and detoxification activities. Cu and Ag metal nanoparticles and Ag/Cu bimetallic nanoparticles used for this purpose can be easily produced on a large scale at low cost and can be applied in many areas. These nanoparticles are among the promising materials due to their surface functional groups. In the literature, experimental studies have been reported on the photodegradation, adsorption and photocatalysis effects of dyes by these nanoparticles [16–18].

The aim of this study is to synthesize stable metallic Ag NPs, Cu NPs, and bimetallic Ag/Cu NPs using the extract of the *Helichrysum arenarium* plant, which is a rarely used aromatic plant, providing on the advantages of green synthesis, such as reduced toxicity by avoiding harmful chemicals, cost-effectiveness using a plant source, and the effect of natural stabilizing agents present in the plant extract. Furthermore, this study aims to utilize the adsorption method with the synthesized nanoparticles to remove MO and MB dyes from aqueous solutions which includes the optimization of adsorption parameters (pH, contact time and adsorbent amount), and to determine both adsorption isotherms, and adsorption kinetics. The results indicate that, under optimum experimental conditions, while MO removal by using Ag/Cu NPs was found to be 76.9% (20 mg/L MO, 20 mg Ag/Cu NPs, 60 min contact time, pH 2), MB removal by using Ag NPs was found to be 82.7% (20 mg/L MB, 20 mg Ag NPs, 60 min contact time, pH 4). The reusability of all nanoadsorbents was performed as three cycles with the same concentration and they can be used after three cycles without losing its efficiency.

Materials and methods

Materials

Silver Nitrate ($AgNO_3$) was purchased from Fluka. Copper (II) sulfate pentahydrate ($CuSO_4{\cdot}5H_2O$) was purchased from Indosaw. Deionized water was used throughout all experimental studies (18.2 MΩ cm). Methyl Orange ($C_{14}H_{14}N_3NaO_3S$) and Methylene Blue($C_{16}H_{18}ClN_3S$) were received from Merck and Fluka.

Instrumentation

Labart SH5 and Heidolph MR 3001 magnetic stirrers were used for mixing and heating processes during the preparation of extract, metallic Ag NPs, metallic Cu NPs, bimetallic Ag/Cu NPs and adsorption experiments. The separation of nanoparticles was made with Hettich Universal 320 Centrifuge. The pH values were controlled with the Thermo Orion 3 Stars pH meter. The morphological and chemical characterizations for nanoparticles were characterized by Thermo Fisher

Scientific Nicolet IS10 ATR-FTIR, Shimadzu UV-1800 UV–Vis Spectrophotometer, Carl Zeiss EVO-LS 10 SEM and TEM-120 kV Transmission Electron Microscope.

Synthesis of nanoparticles

1.0 g of Helichrysum plant was weighed and added to 50 mL of deionized water. This mixture was stirred at 25 °C for 5 h. After mixing, the solid plant residue and the extract were separated from each other with the help of filter paper. At the same time, 0.1 M of 50 mL Silver Nitrate ($AgNO_3$) was prepared, and 5 mL of the plant extract was added to 45 mL of 0.1 M $AgNO_3$ solution to synthesize Ag NPs. On the other hand, 7 mL of plant extract was added to 0.1 M of 50 mL of copper(II) sulfate pentahydrate ($CuSO_4{\cdot}5H_2O$) solution to synthesize Cu NPs. Moreover, 10 mL of plant extract was added to 0.1 M of 100 mL solution including 1.69 g $AgNO_3$ and 2.49 g $CuSO_4{\cdot}5H_2O$ for the synthesis of Ag/Cu NPs. Then, they were mixed with a magnetic stirrer at 500 rpm and kept at room temperature for approximately 30 min to settle. After solid and liquid parts of the obtained nanoparticles were separated by centrifugation, they were washed with deionized water with three times and dried in an oven [16].

Adsorption experiments

Effect of pH on adsorption

The effect of pH on the adsorption of MO and MB onto these NPs was investigated at different pH values of 2, 4, 6 and 8, keeping other parameters as constant (both MO and MB: 20 mg/L; adsorbent amount: 20 mg; contact time: 90 min).

Effect of adsorbent amount on adsorption

For the optimization of the nanoparticle amount, other conditions were kept constant for each nanoparticle according to their type and the adsorbent amounts were changed as 10, 20, 30 and 40 mg in solutions containing 20 mg/L of MO and MB.

Effect of contact time on adsorption

For the optimization of contact time, the experiments were carried out with various contact times of 5, 10, 20, 30, 40, 50, 60, 70, 80, 90, 100, 110, 120, 130, 140 and 150 min while maintaining other conditions constant (20 mg/L of MO and MB solution, 20 mg of adsorbent amount and optimum pH for each NPs).

The adsorption kinetics for MO and MB on nanoparticles were investigated under optimum conditions. The kinetic equations were applied to the experimental data to investigate the potential rate determining step of the adsorption process. Two kinetic models were used as pseudo first order (PFO) equation and pseudo second order (PSO) equation shown in the Eqs. 1 and 2 [17].

The pseudo-first order equation can be expressed as:

$$q_t = q_e \times [1 - \exp(-k_1 t * t)] \quad (1)$$

Here k_1 is the pseudo-first order rate constant (min^{-1}), q_t and q_e are the amount of desired molecules adsorbed at equilibrium and time t. This equation describes a reversible equilibrium between the solution and adsorbent.

The pseudo-second order equation can be expressed as:

$$q_t = \frac{{q_e}^2 \times k_2 \times t}{[k_2 \times q_e \times t] + 1} \quad (2)$$

Here k_2 is the pseudo-second order rate constant (g/mg min), q_t and q_e are the amount of dyes adsorbed at equilibrium and time t [17].

Adsorption isotherms

Adsorption experiments were applied under optimum conditions in 10, 20, 40, 80 and 100 mg/L of MO and MB solutions. The values obtained from UV–Vis Spectrometer measurements and both Langmuir and Freundlich isotherm models were used.

The Langmuir equation can be expressed as:

$$q_e = \frac{q_m \times K_L \times C_e}{1 + K_L \times C_e} \quad (3)$$

Here, q_e (mg/g) is the adsorbed amount per unit mass of the adsorbent, the maximum monolayer adsorption capacity of the adsorbent is q_m (mg/g), and K_L (L/mg) is the Langmuir adsorption constant, C_e (mg/L) is the equilibrium state concentration [17].

The Freundlich isotherm model creates more than one layer on a heterogeneous surface for adsorption.

The Freundlich equation can be expressed as:

$$q_e = K_F {C_e}^{1/n} \quad (4)$$

Here, q_e (mg/g) is the amount of adsorbed per unit mass of the adsorbent, K_F is the Freundlich adsorption constant, C_e (mg/L) is the concentration in equilibrium state. K_F is related to the adsorption capacity of the adsorbent, 1/n, and n (L/mg) represent the constant related to the adsorption intensity [17]. If 1/n is between zero and 1 ($0 < 1/n < 1$), adsorption is considered as convenient. When 1/n is greater than 1, the adsorption process is inconvenient and when $n = 1$, it is irreversible.

Desorption of adsorbed MO and MB on adsorbent surface

Three desorption agents, such as deionized water, 0.1 M HCl, ethanol were used to desorb MO and MB which were adsorbed on Ag NPs, Cu NPs, and Ag/Cu NPs. It was observed that desorption using deionized water provided exceptionally low

dye recovery (Fig. S1). This shows the stability of the adsorption under neutral conditions.

Result and discussion

Characterization

SEM–EDX characterization

As seen in Fig. 1a, the amount of Ag is found to be 58.4%, while the amount of O is found to be 30.5% due to reducing agents from the both salt and extract. As seen in Fig. 1b, the amount of Cu is found to be 31.3%, and the amount of O is found

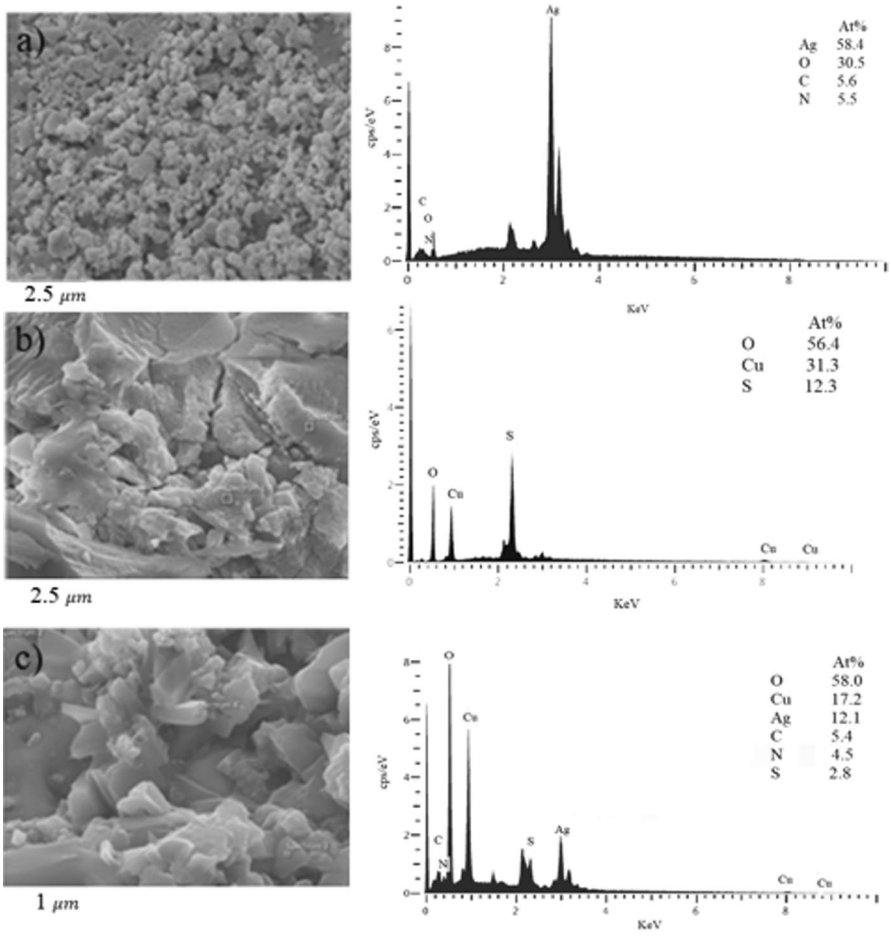

Fig. 1 SEM–EDX of (**a**) Ag NPs (2.5 μx), **b** Cu NPs (2.5 μx) and (**c**) Ag/Cu NPs (1 μx)

to be 56.4% due to reducing agents from the both metal salt and extract. As seen in Fig. 1c, the amounts of Ag, Cu and O are found to be 12.1%, 17.2%, and 58%. Therefore, it can be assumed that the effect of Cu on properties of Ag/Cu NPs is higher than the effect of Ag.

TEM characterization

In the TEM image of Ag/Cu NPs, while the dark parts show Cu NPs, the brighter regions show the Ag NPs, and the structure of Ag/Cu NPs is seen to be stacked and layered shown in Fig. 2c. The images obtained from TEM were calculated using the Image J program and nanoparticle sizes were determined. According to the determined data, Ag NPs, Ag/Cu NPs and Cu NPs were in spherical crystalline structure, monodisperse and the average particle diameters were 14.20 ± 0.20 nm for Ag NPs, 10.25 ± 0.20 nm for Ag/Cu NPs and 5.80 ± 0.10 nm for Cu NPs [16].

FTIR and XRD characterization

The Fig. S2 shows both FT-IR after and before adsorption and XRD results of the nanoparticles after adsorption. According to the results, the shift in peak locations, the peaks given by the functional groups that are not in the content of the nanoparticle but are present in the dyes, the peaks given by the functional groups that create differences between the dyes, and the change in peak intensities confirm that adsorption has been occurred.

The presence of prominent peaks of Ag NPs, Cu NPs and Ag/Cu NPs shown in Fig. S2a–c suggest that biologically active molecules may act as both reducing and stabilizing agents during the formation of NPs. The peak of Ag/Cu NPs at

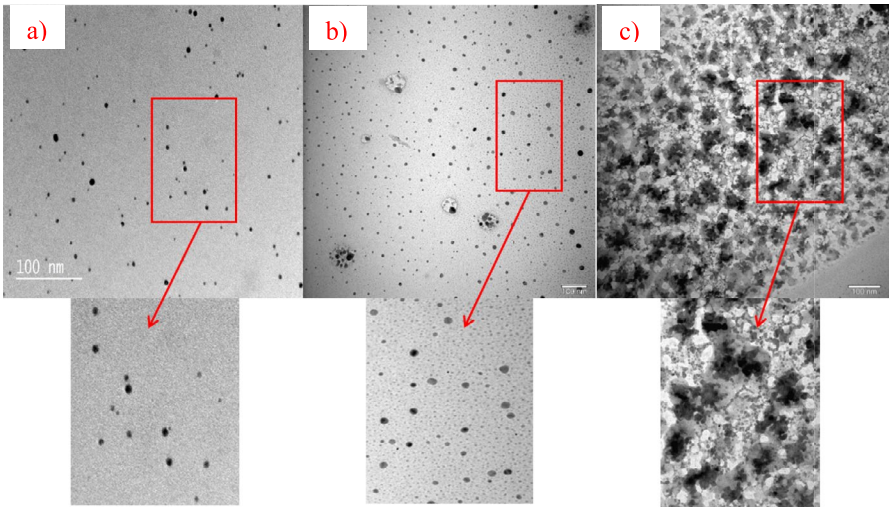

Fig. 2 TEM Images of Nanoparticles (**a**) Ag NPs, (**b**) Cu NPs, (**c**) Ag/Cu NPs (×100 nm)

3385 cm^{-1} shown in Fig. S2b belongs to O–H stretching and bending vibration, while the peaks at 2956 cm^{-1} and 2814 cm^{-1} indicate C–H vibrations. C = O stretching of polyphenols at 1627 cm^{-1}, carboxylate group (COO) stretching at 1454 cm^{-1}, CH bending at 1313 cm^{-1}, CO stretching at 1224 cm^{-1}, C–O stretching vibration at 1082 cm^{-1} and C–H out-of-plane bending vibration at 846 cm^{-1} are also displayed.

There are seven specific peaks at 3392, 1652, 1614, 1514, 1384, 1195 and 1066 cm^{-1} in the FTIR spectra of Cu NPs before and after adsorption shown in Fig. S2c. These peaks represent O–H stretching, C = C stretching, C = C stretching, C = C aromatic ring stretching, C–OH stretching vibrations, C–OH and C–OH bending.

When the FTIR spectrum of Ag NPs before and after adsorption was examined shown in Fig. S2a, some specific peaks at 3375, 2964, 1606, 1421 and 1083 cm^{-1} were found. The peak originating from O–H and N–H stretching is observed at 3375 cm^{-1}. C–H stretching is observed at 2964 cm^{-1}. C = O stretching, C = C stretching and C–N stretching are observed at 1606 cm^{-1}, 1421 cm^{-1} and 1083 cm^{-1}. FTIR analysis revealed that Ag/Cu NPs, Ag NPs and Cu NPs were successfully biosynthesized.

The crystal structures of Ag/Cu NPs, Ag NPs and Cu NPs were characterized by using XRD analysis shown in Fig. S2d. Ag NPs showed five different diffraction zones at 38.1, 44.3, 64.5, 77.4 and 81.6° corresponding to (111), (200), (220), (311) and (222) crystal surfaces. Cu NPs showed diffraction zones at 43.2, 50.4 and 73.9° corresponding to (111), (200) and (220) crystal surfaces. It was determined that XRD analysis data for Ag NPs were compatible with the JCPDS card (01-087-0717) data, while the Cu NPs data were compatible with the JCPDS card (01-070-3038).

Adsorption results

MB is a positive (cationic) dye, and this feature significantly affects its interaction with nanoparticle surfaces, especially in terms of electrostatic forces. The interaction of MB with nanoparticle surfaces is a complex process and may contain multiple mechanisms. If the surface charge of nanoparticles (usually affected by coating agents caused by synthesis or pH) is negative, electrostatic attraction with cationic MB plays an important role [19].

MO is an anionic azo dye containing a sulfonate group and due to this feature, it is negatively charged especially in aqueous solutions above its pK_a value. The sulfonic group in the dye molecule forms the basis of the anionic structure [20].

The optimum pH values were found to be 4 for Ag NPs, 2 for Cu NPs and 4 for Ag/Cu NPs for MB adsorption shown in Fig. 3a. On the other hand, the optimum pH value was found to be 2 for Ag NPs, 2 for Cu NPs, 2 for Ag/Cu NPs for MO adsorption shown in Fig. 3b. At the pH values above 6 especially for MO adsorption, the adsorption efficiency of all NPs decreases considerably because the competition with OH^- ion can reduce the adsorption efficiency. Since the adsorption technique is related to the nanoparticle-dye relationship, the nanoadsorbent surface is an especially important characteristic feature and plays a key role in the efficiency of adsorption. It was determined that the efficiency of adsorption decreases with the increase the solution pH. Therefore, optimum values that were more acidic were

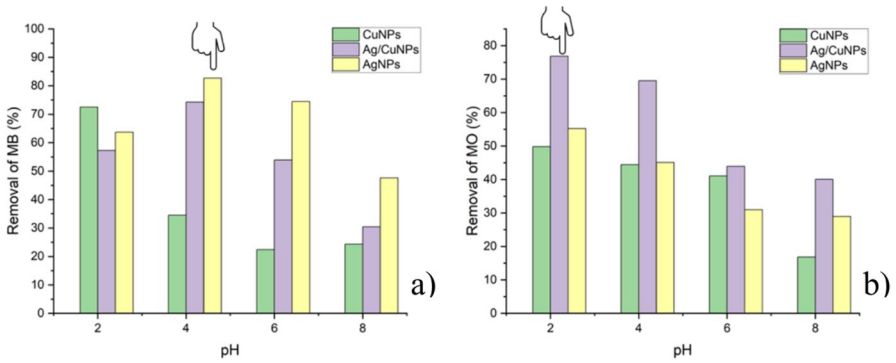

Fig. 3 pH Optimization for (**a**) MB Adsorption and (**b**) MO Adsorption (concentration of both dyes: 20 mg/L; adsorbent amount: 20 mg; contact time: 90 min)

selected for subsequent adsorption experiments. According to experimental results, the optimum pH values for MO adsorption is lower than that MB adsorption. The modifications in adsorbent materials can significantly alter the pH dependence of dye adsorption. The possibility of specific chemical interactions or complex formation between the dye and the adsorbent surface beyond simple electrostatic interactions is also an important advantage of synthesis via green method. The surface charge behaviours of Ag NPs, Ag/Cu NPs and Cu NPs were determined in 0.01 M NaCl medium and pHpzc values were found to be 8.05, 6.07 and 6.09, respectively (Fig. S3). According to these results, the surface of Ag NPs gains a negative charge in more basic conditions, but Ag/Cu NPs and Cu NPs change their surface charge at lower pHs. The fact that Ag/Cu NPs and Cu NPs have similar pHpzc values indicates that Cu metal has a more dominant effect in the bimetallic alloy.

With the values obtained from the UV–Vis measurements, it was found that the reasonable adsorbent amount was found to be 20 mg shown in the Fig. S4.

After optimization studies for the adsorption were performed, it was found that while Ag NPs showed the best adsorption for MB dye, Ag/Cu NPs showed the best adsorption for MO dye. The correlation coefficient numbers and model constants of the PFO and PSO kinetic modelling of the relevant dye and adsorbent are shown in Table 1.

As can be seen from the Table S1, the correlation values of PFO equation kinetic data for MO adsorption are found to be 0.9959 for Ag NPs, 0.9775 for Cu NPs and 0.9953 for Ag/Cu NPs, while the correlation values for PSO equation are found to be 0.9948 for Ag NPs, 0.9815 for Cu NPs, 0.9858 for Ag/Cu NPs. On the other hand, if we look at kinetic data for MB adsorption, the compliance with PFO and PSO equations for Ag NPs are found to be 0.9779 and 0.9913, respectively, while that for Cu NPs are found to be 0.9731 and 0.9868, respectively and that for Ag/Cu NPs are found to be 0.9780 and 0.9625, respectively shown in both Fig. S5 and Table S1. Based on the correlation coefficient values, it can be found that the adsorptions are compatible with physical and/or chemical adsorption. Since the correlation values in PSO equation are higher, the chemical adsorption is the rate-limiting step

Table 1 Kinetic parameters for nonlinear pseudo-first order and pseudo-second order equation

	Pseudo-first order			Pseudo-second order		
Adsorbent-dye	k_1 (min^{-1})	qe (mg g^{-1})	R^2	k_2 (g/mg min)	qe (mg g^{-1})	R^2
Ag/Cu NPs-MO	0.095 ± 0.002	26.793 ± 0.96	0.9953 ± 0.0011	0.01019 ± 0.00089	56.321 ± 0.245	0.9858 ± 0.0011
Ag NPs-MB	0.134 ± 0.002	15.943 ± 0.46	0.9779 ± 0.0009	0.00933 ± 0.00147	18.242 ± 0.051	0.9913 ± 0.0014

for the adsorption of MO and MB on nanoparticles. PSO kinetics generally indicate a stronger interaction involving chemical bonds between the dye and the nanoparticle surface, while PFO kinetics may indicate a more physical adsorption process in which the rate of adsorption is limited primarily by the diffusion of the adsorbate to the surface. The observation of both models indicates that the surface properties and the nature of the dye-adsorbent interactions are sensitive to the synthesis conditions and the specific plant extract used [21]. Since the PFO model is more compatible with the adsorption of the MO dye, it can be assumed that physisorption occurs and there are weak bonds such as Van der Waals and Hydrogen bonds between the dye and the surface of nanoparticles. However, the compatibility of the PSO kinetic model data for the MB dye indicates that chemical adsorption occurs between the adsorbent surface and the molecule surface. This may mean that the adsorption technique involves the formation of covalent bonds between the binding sites of the adsorbent and dye molecules through electron sharing.

According to Langmuir and Freundlich Isotherm Modelling, both equation constants and other parameters obtained are given in the Table 2. It has been concluded that based on interactions between adsorbent and dye, while the compliance with Langmuir or Freundlich isotherms is sometimes effective, sometimes both isotherms are effective shown in Fig. S6. The good fit of both Langmuir and Freundlich isotherms in our adsorption system indicates that the adsorption process is quite complex and cannot be fully described by a single idealized model. This indicates that adsorbent surfaces may exhibit both homogeneous and heterogeneous properties, or that adsorption may involve a combination of both monolayer and multilayer mechanisms. Such behaviour is frequently observed, especially when using natural or slightly processed adsorbents [22]. When the dye and adsorbent interactions are suitable for Langmuir isotherm, it can be considered that the adsorbent surface is homogeneous, the areas are energetically equal, each region adsorbs at most one dye molecule and there is no interaction between the dye molecules in adjacent regions [23]. On the other hand, when that interactions are suitable for Freundlich isotherm, it is assumed that the dye molecules are multilayered in adsorption. In addition, it can be assumed that the adsorbent surface is heterogeneous in terms of adsorption area and surface energy [24].

The constant of Langmuir isotherm (k_L) is an indicator of how strongly adsorbate molecules bind to the active sites on the adsorbent surface. The larger the k_L value, the higher the affinity of the adsorbate to the adsorbent. This means that the adsorbate molecules are more strongly attached to the surface and the adsorption is more favourable [25]. When the lowest k_L values of 0.00542 (Ag/Cu NPs—MO) and the highest k_L value of 0.03443 (Cu NPs—MO) in our data are compared, it means that the affinity and binding energy of the adsorbate to the Cu NPs surface are significantly higher. The adsorbent can hold the adsorbate more effectively, especially at low concentrations. The isotherm curve will show a steeper increase at low concentrations and will tend to reach surface saturation more quickly. The q_{max} values obtained from the Langmuir isotherm were higher for Ag/Cu NPs for both dyes. The surface area values calculated based on the q_{max} values obtained in adsorption typically provide an estimate of the surface properties of the material. The estimated

Table 2 Langmuir and Freundlich adsorption isotherm models for adsorption of MB and MO dyes by all nanoparticles

Adsorbent-Dye	Langmuir isotherm model			Freundlich isotherm model		
	q_{max} (mg/g)	k_L (L/mg)	R^2	k_F (L/g)	n	R^2
Ag/Cu NPs-MO	191.696 ± 10.86	0.00542 ± 0.001	0.97433 ± 0.0051	0.433 ± 0.023	0.8248 ± 0.09	0.98488 ± 0.0041
Ag NPs-MO	88.816 ± 12.21	0.02323 ± 0.006	0.9901 ± 0.0026	4.274 ± 0.326	1.621 ± 0.05	0.99822 ± 0.0022
Cu NPs-MO	59.257 ± 6.36	0.03443 ± 0.008	0.98799 ± 0.0031	4.287 ± 1.115	1.814 ± 0.22	0.97867 ± 0.0023
Ag/Cu NPs-MB	374.001 ± 26.64	0.00662 ± 0.001	0.98484 ± 0.0030	2.876 ± 0.101	1.112 ± 0.12	0.9816 ± 0.0041
Ag NPs-MB	189.210 ± 5.20	0.00961 ± 0.001	0.98903 ± 0.0025	2.653 ± 0.105	1.256 ± 0.15	0.97953 ± 0.0024
Cu NPs-MB	182.226 ± 5.175	0.01104 ± 0.004	0.98072 ± 0.0028	3.334 ± 0.714	1.325 ± 0.09	0.99247 ± 0.0019

surface area obtained using the adsorption data was 914.7 m^2/g for Ag/Cu NPs. The surface areas for other nanoparticles are given in Table S2.

The constant of Freundlich Isotherm (k_F) is related to the adsorption capacity of the adsorbent. Generally, a larger k_F value indicates a larger adsorption capacity. k_F depends on the value of 'n'. The smaller the value of 1/n (and therefore the larger the value of n), the more heterogeneous the surface is adsorbed, and the higher energy sites are filled first, which generally indicates good adsorption [26]. In our experimental data, the value of $n = 1.814$ (and therefore $1/n < 1$) generally indicates a better and more typical adsorption behaviour, while the value of $n = 0.8248$ ($1/n > 1$) indicates more special cases, for example, adsorption where adsorption is initially difficult or where there are strong interactions between the adsorbed molecules. These differences provide important information about the adsorption mechanism and the effectiveness of the adsorbent.

For desorption studies, 0.1 M HCl, pure ethanol and pure water were used for the test of the reusability of nanoparticles. In general, the recovery in pure water was found to be extremely low. Because the acid damaged the structure of the dye, the recovery could not be achieved. On the other hand, the recovery rates of adsorbed dyes in ethanol were varied between 20 and 46% shown in Fig. S1. The remaining dye molecules are stayed on the surface of the adsorbent.

Comparison of method with literature

Cu NPs synthesized by green method in Cynomorium coccineum plant extract showed superior performance in dye adsorption. Adsorption capacity reached at 64 mg/g at room temperature. It showed a strong dye-nano adsorbent interaction. Considering the eco-friendly plant support and good adsorption performances, it was revealed that Cu NPs prepared by green synthesis method can be used for the treatment of polluted waters and can be investigated in other environmental applications [27].

İsmail et al. synthesized Cu NPs by green synthesis method using D. erecta fruit extract. They found that Cu NPs showed extraordinary performance in the catalytic reduction of carcinogenic azo dyes, such as MO and CR, and considering this catalytic performance; the prepared Cu NPs can be synthesized in large quantities and used for the treatment of water due to their low cost, high stability, reusability and environmental friendliness [28].

Ag NPs synthesized by Junejo et al. have been proven to be exceptionally efficient catalysts with improved reduction rate for methyl green (MG) dye. The study has highlighted that Ag NPs can be equally useful for the reduction of other dyes [29].

Rohaizad et al. have synthesized stable Ag NPs using C. roseus extract. The increase in Ag NPs concentration increased the removal percentage of MB. This is because of structure and surface area of Ag NPs. It has been proven that NPs synthesis by green synthesis method can be used in the preparation of other metallic, bimetallic, and metal oxide nanoparticles and their nanocomposites to address the current water pollution problem [30].

Christina et al. prepared Ag/Cu bimetallic nanoparticles using waste Punica grantum bark (PGP) extract. The photocatalytic efficiency of bimetallic nanoparticles was investigated using Congo red dye, showing 100% degradation within 40 min. The results show that maximum degradation was achieved by photocatalysis process. Bimetallic Ag/Cu NPs also have excellent antibacterial effects and can be used to treat bacterial diseases. As a result, it was observed that these catalysts have a wide range of applications for nature, especially effective in photocatalytic properties of organic dyes and pollutants [31].

Table 3 presents the q_{max} values, adsorption efficiencies, and compatible isotherm and kinetic models for the nanoparticles investigated in our study, alongside those of nanoparticles and nanoparticle composites reported in other studies.

Conclusion

In this study, the adsorption of MO and MB dyes in aqueous medium onto Ag/Cu NPs, Cu NPs and Ag NPs obtained by green synthesis method was studied. Two classical isotherm models were examined. The isotherm parameters that best fit the experimental data vary according to the adsorbent and adsorbate. According to the models, it mostly conforms to the Langmuir isotherm. Accordingly, the adsorption increases linearly with the initial concentration of the dye. When the surface is covered with a single layer and the amount of adsorbate adsorbed on the adsorbent surface remains constant, the maximum saturation point of adsorption is reached. The adsorption rate is directly proportional to the adsorption areas on the adsorbent surface and the adsorbate concentration. While the q_{max} values were found to be 88.816 mg/g for Ag NPs, 59.257 mg/g for Cu NPs, 191.696 mg/g for Ag/Cu NPs for MO dye, that were found to be 189.210 mg/g for Ag NPs, 182.226 mg/g for Cu NPs, 374.001 mg/g for Ag/Cu NPs for MB dye. Although the optimum pH values changed with the adsorbent-adsorbate compatibility, pH 4 provided the optimum conditions. For the amount of adsorbent, the 20 mg value was chosen as optimum because there were no dramatic differences with both 30 mg and 40 mg but there was a significant difference against to 10 mg value. After these parameters were fixed, both the contact time and the kinetic parameters were examined, and it was found that the adsorption reached maximum saturation at the between 60 and 90 min. While MO was compatible with the PFO kinetic model, MB was compatible with the PSO kinetic model. In desorption studies, pure water could not recover dyes, while acid also damaged the structure of dyes, but ethanol provided recovery between 20 and 30%. However, the optimization experiments for desorption studies were not performed because extremely low amounts of removal would be provided when adsorption was tried again. While Ag/Cu NPs provided 76.9% removal for MO, both Ag NPs

Table 3 Recent studies about MO and MB dye adsorption with different adsorbents

Types of Adsorbents	Dye	q_{max} (mg/g or mmol/g)	Adsorption efficiency	Isotherm models	Kinetic model	Refs
Ag NPs, Cu NPs and Ag/Cu NPs from *Helichrysum Arenarium*	MB/MO	Ag NPs MO 88.816 mg/g; MB 189.21 mg/g	55% 82.7%	Langmuir	PSO for MB PFO for MO	This study
		Cu NPs MO 59.257 mg/g; MB 182.226 mg/g	49% 72.5%			
		Ag/Cu NPs MO 191.696 mg/g; MB 374.001 mg/g	77% 74.3%			
Ag NPs from *Salvinia molesta*	MB	121.04 mg/g	(> 95%)	Langmuir	PSO	[32]
CuO NPs from *Aloe barbadensis*	MB	95.5 mg/g	98.89%	Langmuir	PFO	[33]
Ophiorrhiza mungos-Mediated Ag NPs	MB	80.451 mg/g	88.1 ± 1.74%	Langmuir	PSO	[34]
Ag NPs from Achillea Tenuifolia	MO	90.90 mg/g	94%	Langmuir	PSO	[35]
Ag NPs from Urena lobata leaf extract	MB	218.95 mg/g	87.47 ± 0.12%	Langmuir	PFO	[36]
Lemon peels activated with phosphoric acid (ALP) and alginate (ALP/A beads)	MB	ALP/A 841.4 mg/g; ALP 208.6 mg/g	80.5 and 70% (6 cycles)	Langmuir	PFO-PSO	[37]
Unmodified citrus peels (UCP) and UCP encapsulated with calcium alginate (UCP/A)	MB	UCP/A 964.54 mg/gUCP 185.83 mg/g	93.6%	Langmuir	Thomas model, Yoon and Nelson model	[38]
Cellulose-based modified citrus peels (CPAA)/calcium alginate composite (CPAA-A)	MB	CPAA-A 923 mg/g; CPAA 200 mg/g	80 and 75% (6 cycles)	Langmuir	CPAA-A PFO CPAA PSO	[39]
Hybrid activated bentonite–alginate composite (ABent/A)	MB	780 mg/g	High desorption efficiency (> 90%, 6 cycle)	Langmuir	PFO	[40]

Table 3 (continued)

Types of Adsorbents	Dye	q_{max} (mg/g or mmol/g)	Adsorption efficiency	Isotherm models	Kinetic model	Refs
TiO_2/activated carbon from rice husk	MB/MO	0.452 mmol/g; 0.329 mmol/g	Great performance	Langmuir	PFO	[41]
Biochar derived from date palm petioles powder (DPB)/date palm petioles (DPP)	MO	DPB 514.79 mg/g; DPP 256.207 mg/g	50–80% adsorption–desorption (3 cycle)	Langmuir	PSO	[42]
Porous carbon material prepared from potassium citrate	MB/MO	1929.38 mg/g; 446.43 mg/g	Higher selectivity for MB compared to MO	Langmuir	PSO	[43]
Triptycene-based hyper-crosslinked porous polymer	MB/MO	159.80 mg/g; 220.82 mg/g	> 80% removal (5 cycle)	Langmuir	PSO	[44]

and Cu NPs could provide 55% and 49% removal, respectively. For MB removal, Ag NPs, Cu NPs, and Ag/Cu NPs provided 82.7%, 72.5% and 74.3% efficiency. In addition, it is seen that Ag/Cu NPs has significant potential in the adsorption of MB and MO dyes from aqueous media. It is concluded that because bimetallic Ag/Cu NPs obtained from natural plant extract, has highly efficient, has not toxic properties due to obtained with green synthesis method and can carry the different properties of Ag NPs and Cu NPs, they can be used as an important alternative to costlier adsorbent materials.

Supplementary Information The online version contains supplementary material available at https://doi.org/10.1007/s11144-025-02874-4.

Data availability Not applicable.

References

1. Aigbe UO, Ukhurebor KE, Onyancha RB, Osibote OA, Darmokoesoemo H, Kusuma HS (2021) Fly ash-based adsorbent for adsorption of heavy metals and dyes from aqueous solution: a review. J Mater Res Technol 14:2751–2774
2. Singh NB, Nagpal G, Agrawal S (2018) Water purification by using adsorbents: a review. Environ Technol Innov 11:187–240
3. Gambhir RS, Sohi RK, Bansal V, Nirola A, Randhawa AK, Sogi GM, Veeresha KL (2013) Newer water purification techniques—a review. Indian J Public Health Res Dev 4(1):249
4. Punia P, Naagar M, Chalia S, Dhar R, Ravelo B, Thakur P, Thakur A (2021) Recent advances in synthesis, characterization, and applications of nanoparticles for contaminated water treatment—a review. Ceram Int 47(2):1526–1550
5. Urucu OA, Garosi B, Musah RA (2025) Efficient phytoremediation of methyl red and methylene blue dyes from aqueous solutions by *Juncus effusus*. ACS Omega 10:1943–1953
6. Ihaddaden S, Aberkane D, Boukerroui A, Robert D (2022) Removal of methylene blue (basic dye) by coagulation-flocculation with biomaterials (bentonite and Opuntia ficus indica). J Water Process Eng 49:102952
7. Othmani B, Gamelas JA, Rasteiro MG, Khadhraoui M (2020) Characterization of two cactus formulation-based flocculants and investigation on their flocculating ability for cationic and anionic dyes removal. Polymers 12(9):1964
8. Bani-Atta SA, Darwish AAA, Shwashreh L, Alotaibi FA, Al-Tweher JN, Al-Aoh HA, El-Zaidia EFM (2024) Efficient photocatalytic degradation of methylene blue and methyl orange using calcium-polyoxometalate under ultraviolet irradiation. Processes 12(12):2769
9. Majeed A, Ibrahim AH, Al-Rawi SS, Iqbal MA, Kashif M, Yousif M, Hussain SA (2024) Green organo-photooxidative method for the degradation of methylene blue dye. ACS Omega 9(10):12069–12083
10. Makhesana MA, Patel KM, Nyabadza A (2024) Applicability of nanomaterials in water and wastewater treatment: a state-of-the-art review and future perspectives. Mater Today Proc. https://doi.org/10.1016/j.matpr.2024.01.037
11. Gebreslassie YT, Gebremeskel FG. (2024). Green and cost-effective biofabrication of copper oxide nanoparticles: exploring antimicrobial and anticancer applications. Biotechnol Rep e00828.
12. Ying S, Guan Z, Ofoegbu PC, Clubb P, Rico C, He F, Hong J (2022) Green synthesis of nanoparticles: current developments and limitations. Environ Technol Innov 26:102336
13. Jadoun S, Arif R, Jangid NK, Meena RK (2021) Green synthesis of nanoparticles using plant extracts: a review. Environ Chem Lett 19(1):355–374
14. Şahin M, Arslan Y, Tomul F, Akgül F, Akgül R (2024) Green synthesis of metal nanoparticles from codium macroalgae for wastewater pollutants removal by adsorption. CLEAN—Soil Air Water 52:2300187

15. Hano C, Abbasi BH (2021) Plant-based green synthesis of nanoparticles: production, characterization, and applications. Biomolecules 12(1):31
16. Şahin M, Arslan Y, Soyuçok A (2024) Helichrysum arenarium-mediated facile green synthesis, antibacterial, catalytic activity, and hydrogen evolution of metallic (Ag, Cu) and bimetallic (Ag/Cu) nanoparticles. Mater Chem Phys 314:128853
17. Güney BC, Arslan Y (2023) Removal of Cu (II) by biopolymer-clay nanocomposite adsorbent. Reac Kinet Mech Cat 136(1):433–448
18. Kahraman HT (2024) Synthesis of silver nanoparticles using *Alchemilla vulgaris* and *Helichrysum arenarium* for methylene blue and 4-nitrophenol degradation and antibacterial applications. Biomass Convers Biorefin 14:1–12
19. Saputra E, Saputra R, Nugraha MW, Irianty RS, Utama PS (2018) Removal of methylene blue from aqueous solution using spent bleaching earth. IOP conference series: materials science and engineering, vol 345. IOP Publishing, Bristol, p 012008
20. Chen G, Yin Y, Zhang X, Qian A, Pan X, Liu F, Li R (2024) Enhanced adsorption of methyl orange from aqueous phase using chitosan-palmer amaranth Biochar composite microspheres. Molecules 29(8):1836
21. Liu B, Luo H, Rong H, Zeng X, Wu K, Chen Z, Xu D (2019) Temperature-induced adsorption and desorption of phosphate on poly (acrylic acid-co-N-[3-(dimethylamino) propyl] acrylamide) hydrogels in aqueous solutions. Desalin Water Treat 160:260–267
22. Mohamad Said KA, Mohamed Amin MA, Yakub I, Rahman MR, Hong Kueh AB, Hamdan S, Rahman MM (2023) Methylene blue adsorption mechanism onto palm kernel shell-derived activated carbon: from particle diffusion to site adsorption. BioResources 18(3):5120–5132
23. Alafnan S, Awotunde A, Glatz G, Adjei S, Alrumaih I, Gowida A (2021) Langmuir adsorption isotherm in unconventional resources: applicability and limitations. J Petrol Sci Eng 207:109172
24. Chung HK, Kim WH, Park J, Cho J, Jeong TY, Park PK (2015) Application of Langmuir and Freundlich isotherms to predict adsorbate removal efficiency or required amount of adsorbent. J Ind Eng Chem 28:241–246
25. Fatima SS, Borhan A, Ayoub M, Ghani NA (2023) Modeling of CO_2 adsorption on surface-functionalized rubber-seed shell activated carbon: isotherm and kinetic analysis. Processes 11(10):2833
26. Nandiyanto ABD, Al Husaeni DN, Ragadhita RISTI, Fiandini MELI, Al Husaeni DF, Maryanti RINA (2023) Analysis of adsorption isotherm characteristics for removing curcumin dyes from aqueous solutions using avocado seed waste carbon microparticles accompanied by computational calculations. J Eng Sci Technol 18(1):706–720
27. Sebeia N, Jabli M, Ghith A, Saleh TA (2020) Eco-friendly synthesis of *Cynomorium* coccineum extract for controlled production of copper nanoparticles for sorption of methylene blue dye. Arab J Chem 13(2):4263–4274
28. Ismail M, Gul S, Khan MI, Khan MA, Asiri AM, Khan SB (2019) Green synthesis of zerovalent copper nanoparticles for efficient reduction of toxic azo dyes congo red and methyl orange. Green Process Synth 8(1):135–143
29. Junejo Y, Baykal A, Safdar M, Balouch A (2014) A novel green synthesis and characterization of Ag NPs with its ultra-rapid catalytic reduction of methyl green dye. Appl Surf Sci 290:499–503
30. Rohaizad A, Shahabuddin S, Shahid MM, Rashid NM, Hir ZAM, Ramly MM, Aspanut Z (2020) Green synthesis of silver nanoparticles from *Catharanthus roseus* dried bark extract deposited on graphene oxide for effective adsorption of methylene blue dye. J Environ Chem Eng 8(4):103955
31. Christina B, Thanigaimani K, Sudhakaran R, Mohan S, Arumugam N, Almansour AI (2024) Green waste immobilized Ag/Cu feather like Bi-matrix on garment dye decomposes and their bio-efficacy. Environ Res 242:117761
32. Batool M, Daoush WM, Hussain MK (2022) Dye sequestration using biosynthesized silver nanoparticles adsorbent in aqueous solutions. Crystals 12(5):662
33. Thakur P, Kumar V (2019) Kinetics and thermodynamic studies for removal of methylene blue dye by biosynthesize copper oxide nanoparticles and its antibacterial activity. J Environ Health Sci Eng 17:367–376
34. Akhi AA, Hasan A, Saha N, Howlader S, Bhattacharjee S, Dey K, Ganguli S (2024) *Ophiorrhiza* mungos-mediated silver nanoparticles as effective and reusable adsorbents for the removal of methylene blue from water. ACS Omega 9(4):4324–4338
35. Yari A, Yari M, Sedaghat S, Delbari AS (2023) Biosynthesis of silver nanoparticles from *Achillea tenuifolia* aqueous flower extract and its application for the efficient removal of acid red 18

and methyl orange from aqueous media: Isotherm and kinetics studies. Iran J Chem Chem Eng 42:3208–3223
36. Gowda SA, Goveas LC, Dakshayini K (2022) Adsorption of methylene blue by silver nanoparticles synthesized from *Urena lobata* leaf extract: kinetics and equilibrium analysis. Mater Chem Phys 288:126431
37. Aichour A, Zaghouane-Boudiaf H, Iborra CV, Polo MS (2018) Bioadsorbent beads prepared from activated biomass/alginate for enhanced removal of cationic dye from water medium: kinetics, equilibrium and thermodynamic studies. J Mol Liq 256:533–540
38. Aichour A, Zaghouane-Boudiaf H, Zuki FBM, Aroua MK, Ibbora CV (2019) Low-cost, biodegradable and highly effective adsorbents for batch and column fixed bed adsorption processes of methylene blue. J Environ Chem Eng 7(5):103409
39. Aichour A, Zaghouane-Boudiaf H (2020) Single and competitive adsorption studies of two cationic dyes from aqueous mediums onto cellulose-based modified citrus peels/calcium alginate composite. Int J Biol Macromol 154:1227–1236
40. Aichour A, Zaghouane-Boudiaf H (2020) Synthesis and characterization of hybrid activated bentonite/alginate composite to improve its effective elimination of dyes stuff from wastewater. Appl Water Sci 10(6):1–13
41. Tu NTT, Thanh TS, Quy PT, Ha TTM, Thu PTK, Bich NH, Khieu DQ (2023) Trinary component adsorption of methylene blue, methyl orange, and methyl red from aqueous solution using TiO2/activated carbon. Adsorpt Sci Technol 2023:8943198
42. Aichour A, Zaghouane-Boudiaf H, Khodja HD (2022) Highly removal of anionic dye from aqueous medium using a promising biochar derived from date palm petioles: characterization, adsorption properties and reuse studies. Arab J Chem 15(1):103542
43. Wang S, Dou J, Zhang T, Li S, Chen X (2023) Selective adsorption of methyl orange and methylene blue by porous carbon material prepared from potassium citrate. ACS Omega 8(38):35024–35033
44. He Y, Bao W, Hua Y, Guo Z, Fu X, Na B, Liu H (2022) Efficient adsorption of methyl orange and methyl blue dyes by a novel triptycene-based hyper-crosslinked porous polymer. RSC Adv 12:5587–5594